Geophysical Research Letters

Supporting Information for

Abyssal Pathways and the Double Silica Maximum in the Northeast Pacific Basin

Susan L. Hautala[1] and Douglas E. Hammond[2]

[1]University of Washington.

[2]University of Southern California.

Contents of this file

A. Lagrangian trajectory tracer initialization values (Figure S-A1).
B. Additional model fields (Figures S-B1, S-B2).
C. Additional model-data comparisons (Figure S-C1).
D. Sensitivity experiment (Table S-D1, Figures S-D1 through S-D5).

Introduction

This supplement contains information about the boundary conditions (supplemental to Figure 1), along with additional model fields and comparisons to observations (supplemental to Figures 1-3).

The final section (D) contains a detailed discussion of the sensitivity experiments that were summarized in the text, with additional supporting figures.

A. LAGRANGIAN TRAJECTORY TRACER INITIALIZATION VALUES

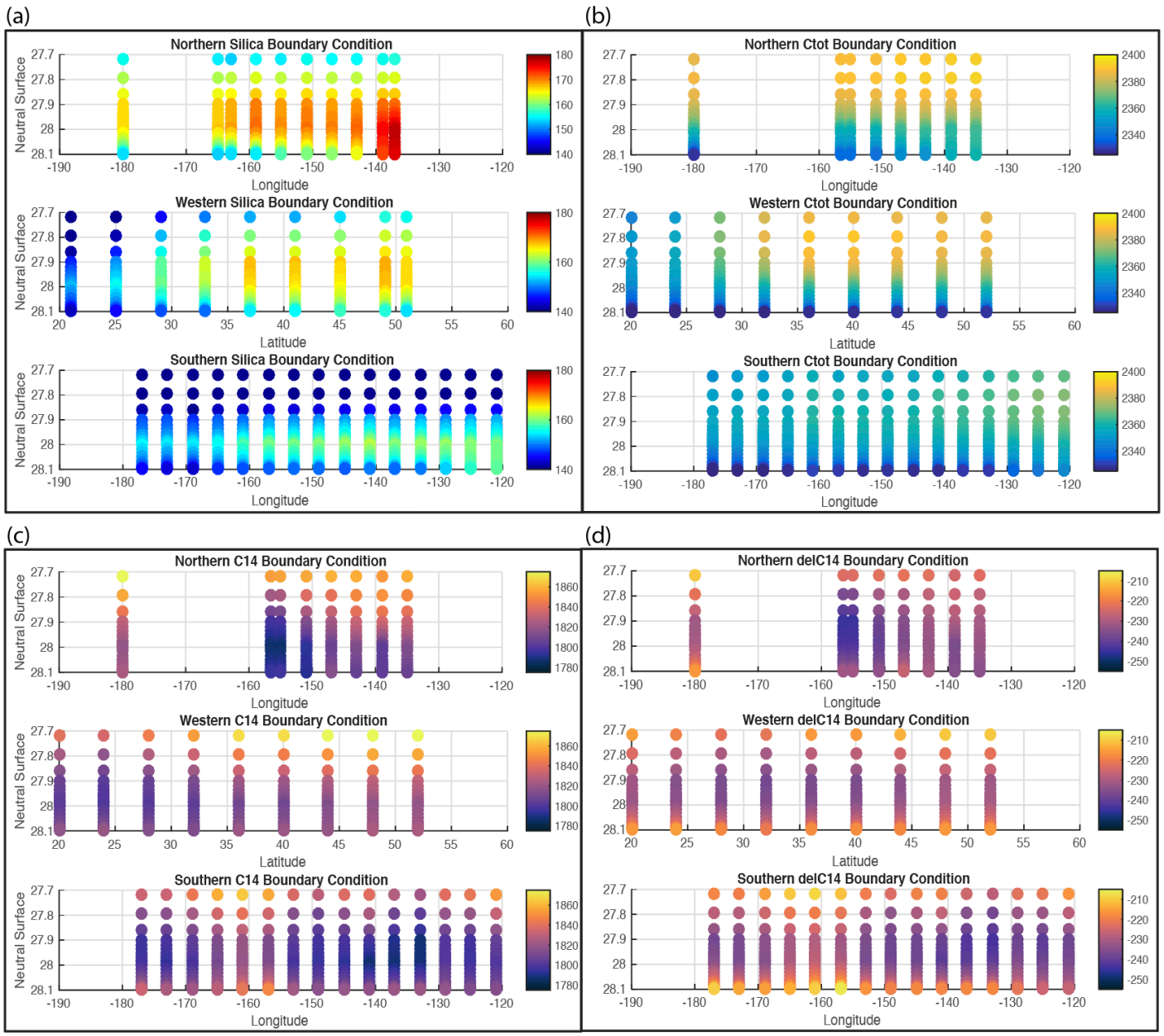

Figure S-A1. Tracer concentration boundary conditions for water parcel trajectories initialized along northern, western, and southern lines: (a) Silica (μmol kg^{-1}), (b) total Carbon (μmol kg^{-1}), (c) ^{14}Carbon normalized by $^{14}C/^{12}C$ ratio in 1950 atmosphere (μmol kg^{-1}), (d) $\Delta^{14}C$ (‰), calculated from (b) and (c).

B. ADDITIONAL MODEL FIELDS

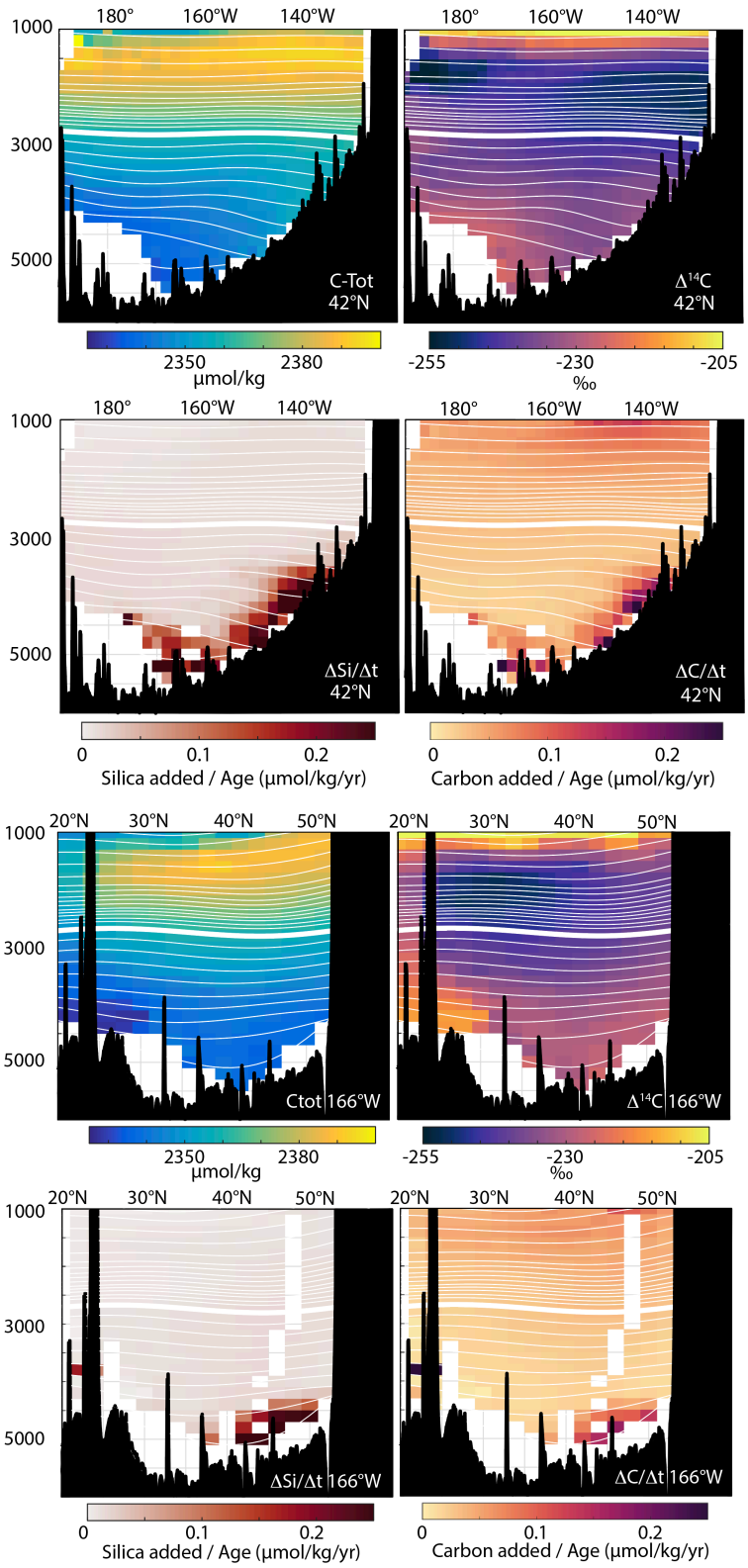

Figure S-B1. Additional bin-averaged tracer fields, as labelled. Tracer added is the value for a Lagrangian water parcel found at a given location minus its initial value. Thus, the rates in the lower panels average the time history of Lagrangian parcels found at a given location, and should not be interpreted as a local (Eulerian) flux rate.

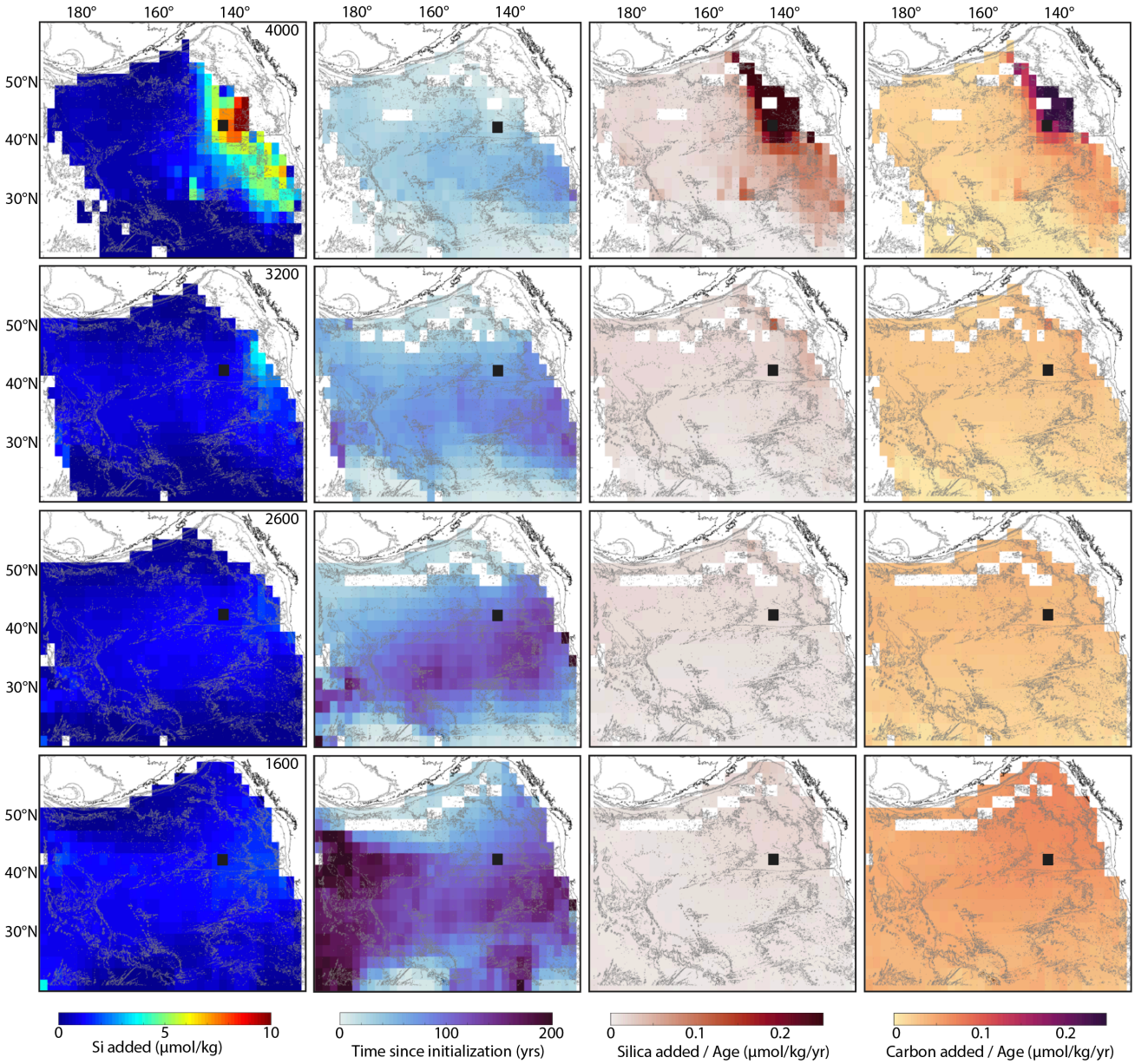

Figure S-B2. Additional bin-averaged variables, on pressure (dbar) surfaces as labelled. The black square marks 42°N, 142°W. Tracer added is the value for a Lagrangian water parcel found at a given location minus its initial value. Thus, the rates in the last two columns average the time history of Lagrangian parcels found at a given location, and should not be interpreted as a local (Eulerian) flux rate.

C. ADDITIONAL MODEL DATA COMPARISONS

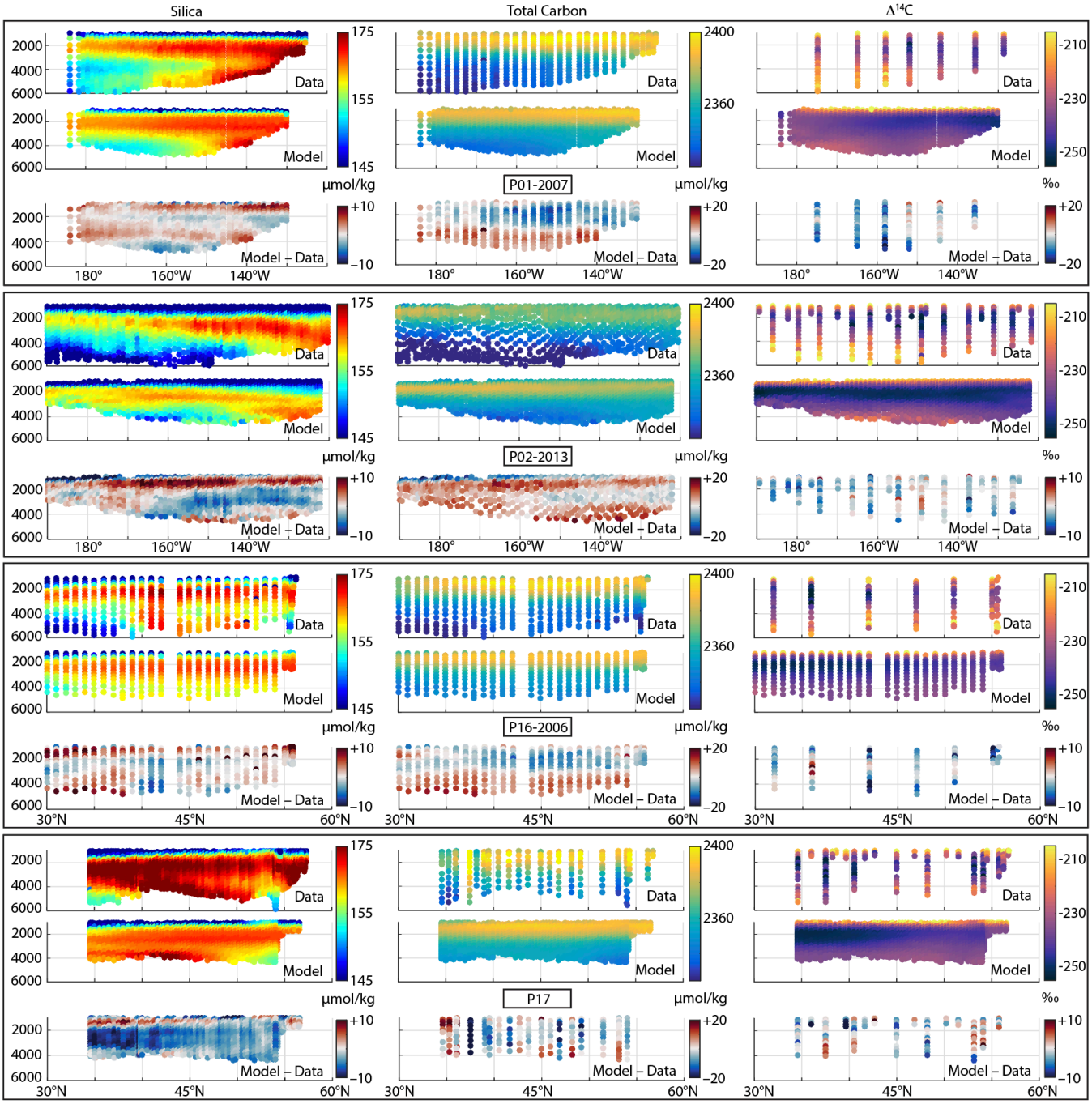

Figure S-C1. Modeled tracer fields interpolated to bottle data locations from hydrographic sections and the model concentration difference from the data. Note that because it is constrained to the UCDW, the model fields do not extend into topographically disconnected pools of denser LCDW in the north and south NEPB. Top row: P01-2007 along nominal 47°N; 2nd row: P02-2013 along ~30°N; 3rd row: P16-2006 along ~150°W; bottom row: P17 along ~135°W but angling to 160°W in the subarctic gyre.

D. SENSITIVITY EXPERIMENTS

Systematic variations to the assumed parameters were explored using 25 realization runs as listed in Table S-D1. It was found that the average radiocarbon bias, relative to the four sections of bottle data, was the most sensitive to variations of the lateral diffusivity, K_H, because of this tracer's inherent decay-related clock. In each case, a new inverse model solution (following Hautala 2018) was computed (Figure S-D3), where the value of lateral diffusivity was specified rather than solved for. As K_H is varied, the magnitude of the radiocarbon bias is affected in opposite sense to the magnitude of the silica bias, and also to RMS misfits to the potential vorticity and salinity constraints in the inverse calculation (Figure S-D1), providing a means of selecting this parameter. A final choice was made by considering the improved radiocarbon agreement with increasing K_H, traded off against the size of the estimated 95% confidence limit error bars for any neutral surface (± 211 m^2/s) for the inverse solution of Hautala (2018), as well as the adverse impact of increasing K_H on silica bias and inverse model misfit. The existence of the double silica maximum is not dependent on this choice (Figure S-D5). A 100-realization version with the parameters of Run 7 (K_H = 260 m^2/s) is interpreted in the main paper. For this solution, the radiocarbon bias is approximately 1% between 1500-3500 m depth, comparable to the error level in deVries et al. (2019). A run that halts trajectories when they dead-end at topographic holes, rather than implementing the "boundary slippage" algorithm (Figure S-D4, compare to Figure 1) loses a great deal of information, especially in the deeper UCDW. However, again the double silica maximum still occurs.

Run	σ km	$K_H = 1/2\ \sigma^2/\Delta t$ m^2/s	Si_Benthic x [20, 200, 600] $mmol/m^2/yr$	Si_Rain x [1, 10, 90] $mmol/m^2/yr$	CB_Source *H* value (m)	Si Added (Tmol) /ΔSi/Δt (Tmol/y) 1000-2800	Si Added (Tmol) /ΔSi/Δt (Tmol/y) 2800-5000
1	40	51	[1,1,1]	[1,1,1]	0	55.8 / 0.33	58.3 / 1.96
2	50	81	[1,1,1]	[1,1,1]	0	51.9 / 0.34	62.8 / 2.00
3	60	116	[1,1,1]	[1,1,1]	0	45.9 / 0.35	53.5 / 1.83
4	70	158	[1,1,1]	[1,1,1]	0	39.0 / 0.34	42.4 / 1.55
5	80	206	[1,1,1]	[1,1,1]	0	33.3 / 0.34	41.0 / 1.54
6	85	232	[1,1,1]	[1,1,1]	0	30.9 / 0.34	38.0 / 1.57
7*	90	260	[1,1,1]	[1,1,1]	0	28.3 / 0.34	32.8 / 1.48
8	100	322	[1,1,1]	[1,1,1]	0	24.5 / 0.37	29.5 / 1.48
9	90	260, no KV	[1,1,1]	[1,1,1]	0	28.6 / 0.34	35.9 / 1.38
10	90	260	[1,1,1]	[1,1,1]	10	51.4 / 0.53	37.2 / 1.67
11	90	260	[1,1,1]	[1,1,1]	50	34.4 / 0.39	32.5 / 1.41
12	90	260	[1,1,1]	[1,1,1]	100	31.5 / 0.36	33.3 / 1.45
13	90	260	[1,1,2]	[1,1,0.5]	0	15.9 /0.19	49.4 / 2.44
14	90	260	[1,2,1]	[1,0.5,1]	0	27.0 / 0.33	33.9 / 1.46
15	90	260	[1,2,2]	[1,0.5,0.5]	0	14.8 / 0.18	47.5 / 2.67
16	90	260	[1.05,1.05,1.15]	[0,0,0]	0	1.0 / 0.02	22.0 / 1.19
17	90	260	[1,1,1]	[1,1,0.33]	0	11.0 / 0.13	27.5 / 1.25
18	90	260	[0,0,0]	[1,1,1]	0	26.6 / 0.32	12.6 / 0.29

Table S-D1. Sensitivity study parameters using 25 realization averages. The total addition of silica in NPDW and UCDW layers during one pass of the water parcels through the basin is reported in the final two columns. Note that for Run 7, a 100 realization run is discussed in the text, leading to minor differences in the values mentioned there.

Random Gaussian displacement:
Runs 1-8 explored the effects of varying the value of the lateral (along neutral surface) displacement after each time step (equivalently, K_H). Larger values of lateral diffusivity increase the misfit in the potential vorticity and salinity conservation equations that are the basis of the circulation inverse model (Figure S-D1 top left). As a final experiment (Run 9), the diapycnal displacement (corresponding to K_V) is set to zero, with only minor impact on bias. The existence of the double silica maximum structure does not depend on the selected value of K_H although the concentration of the near-bottom maximum is reduced as K_H is increased.

Cascadia Basin source:
Runs 10-12 explored the addition of a Cascadia Basin source. If, after a given time-step, a trajectory point was located east of 132°W, between 44°N and 48°N and between 2100 to 2700 dbar, the silica flux was augmented by 0.81 mmol/m^2/yr (Esther et al. 2010), divided by a (boundary layer) height indicated in the 6th column of Table S-D1, converted to μmol/kg/yr. Adding the most extreme version of the Cascadia Basin source (dividing the total flux by the smallest vertical layer thickness (10 m) modestly improved the basin wide average Si bias, particularly improving agreement along P17 for the mid-depth maximum (Figure S-D2).

Silica source function:
Runs 13-17 explored modifications of aspects of the silica source function. While the total amount of silica (right columns of Table S-D1) is impacted, there is little change in basin-average bias (Figure S-D1). Because silica tends to be biased low below 2000 m and biased high above that level, we explored increasing the bottom source in the transitional and subarctic bands separately and then together while halving the water column source. Next (Run 16), we set the water column source to zero and increased the bottom source proportionally. In Run 17, we set the subarctic water column source to 5% of the bottom source (the same percentage as the other latitude bands). Finally (Run 18), we set the bottom source to zero. Although the total amount of silica added to the basin is impacted by changes in source fluxes as expected (Table S-D1), there is no particular improvement in bias relative to Run 7 (Figure S-D1).

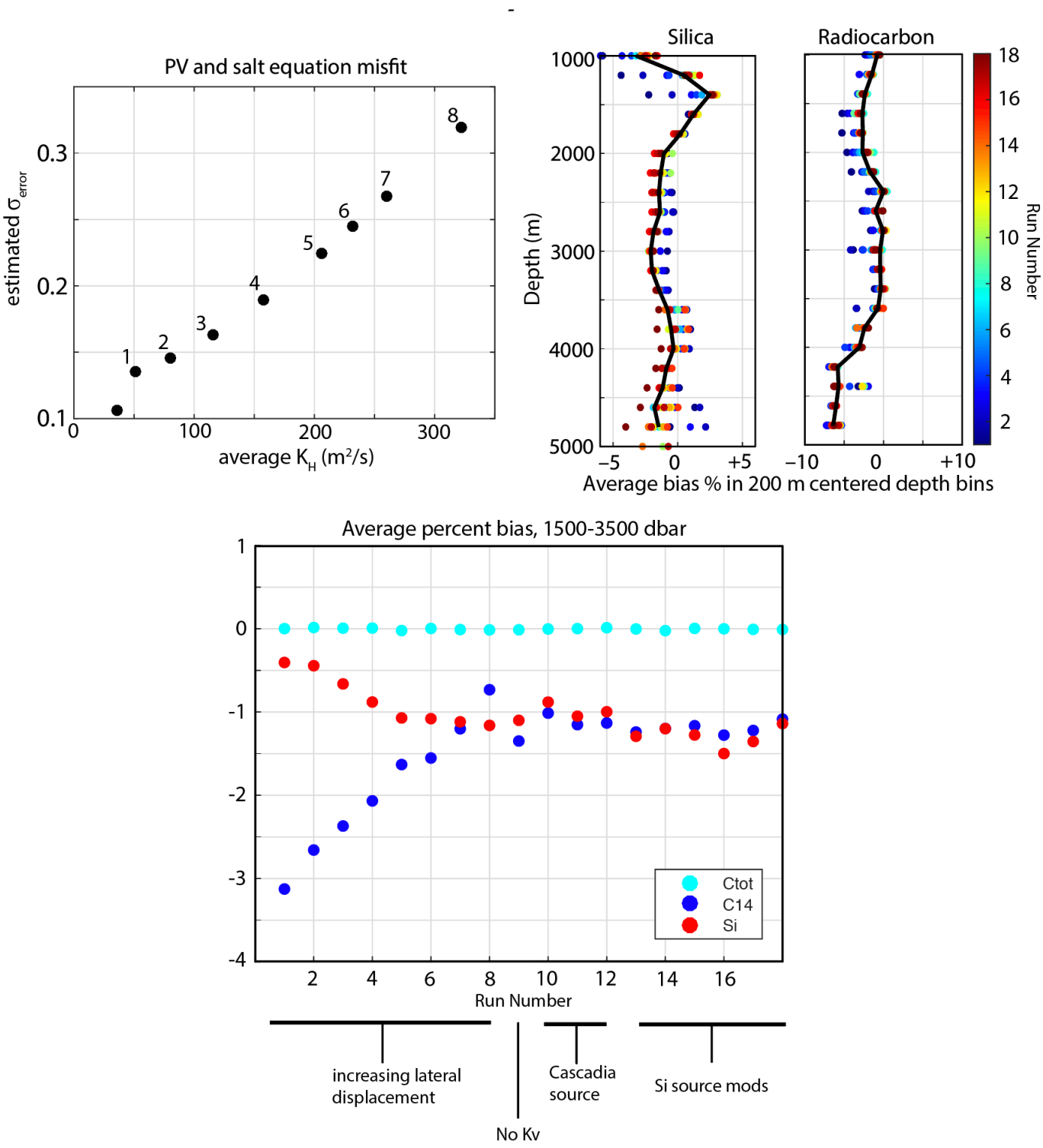

Figure S-D1. Top left: RMS error standard deviation from the inverse fit to potential vorticity and salinity equations using specified values of lateral diffusivity. The left-most data point corresponds to the solution in Hautala (2018) which has a depth-averaged K_H = 36 m^2/s. Values for sensitivity run numbers (Table S-D1) are indicated next to the points. *Top right*: Average percent bias for silica and radiocarbon as a function of depth (compared to the four repeat hydrography sections discussed in the main text) colored by run number. *Bottom*: Average percent bias for 1500-3500 m as a function of run number for each of the three simulated tracers.

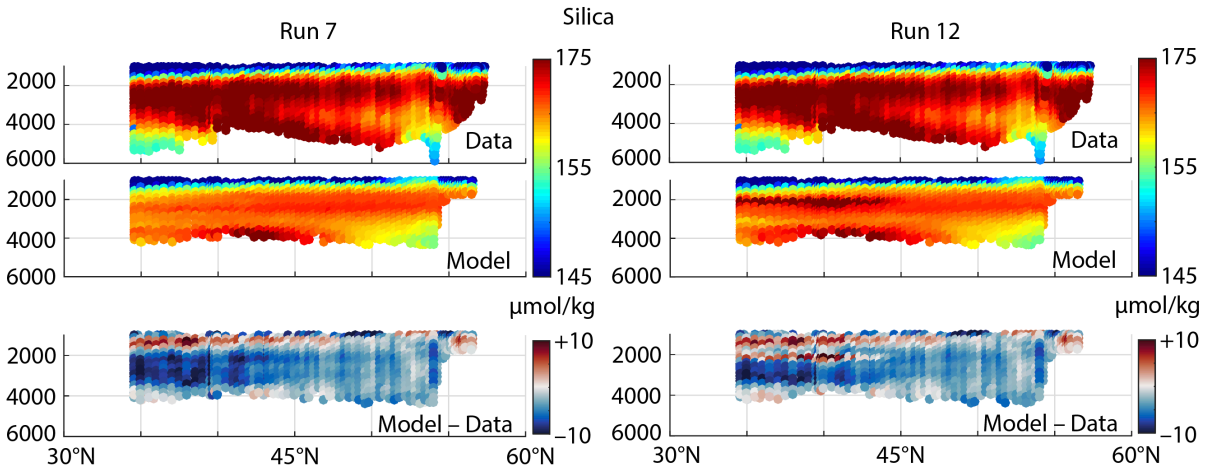

Figure S-D2. Model-data comparison along P17 without (Run 7) and with (Run 12) a crude Cascadia Basin silica source. Of the three experiments with this additional source, Run 12 distributes the estimated seafloor source from Esther et al. (2010) over the smallest depth range (10 m, see Table S-D1) and thus has the greatest impact on concentration.

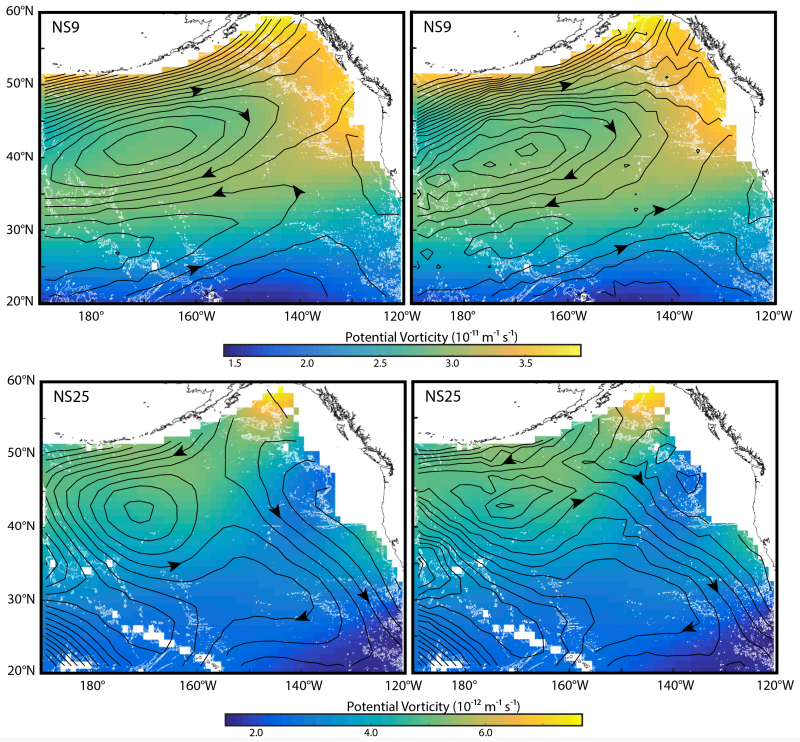

Figure S-D3. Left: Inverse model flow fields and potential vorticity where the lateral diffusivity is solved for as a least-squares fit to potential vorticity and salinity conservation equations (Hautala 2018). *Right:* Flow and potential vorticity from an inverse solution where lateral diffusivity is specified at K_H = 260 m^2/s (Run 7 value). Potential vorticity is colored and absolute geostrophic streamfunction is contoured in black (by 0.02 m^2/s^2) with flow directions indicated. *Top*: γ = 27.795 kg m^{-3}, lying in the middle of the NPDW. *Bottom*: γ = 28.072 kg m^{-3}, lying in the middle of the UCDW. Increased misfit in the potential vorticity and salinity equations with increasing lateral diffusivity manifests as noise in the right panel streamfunction contours.

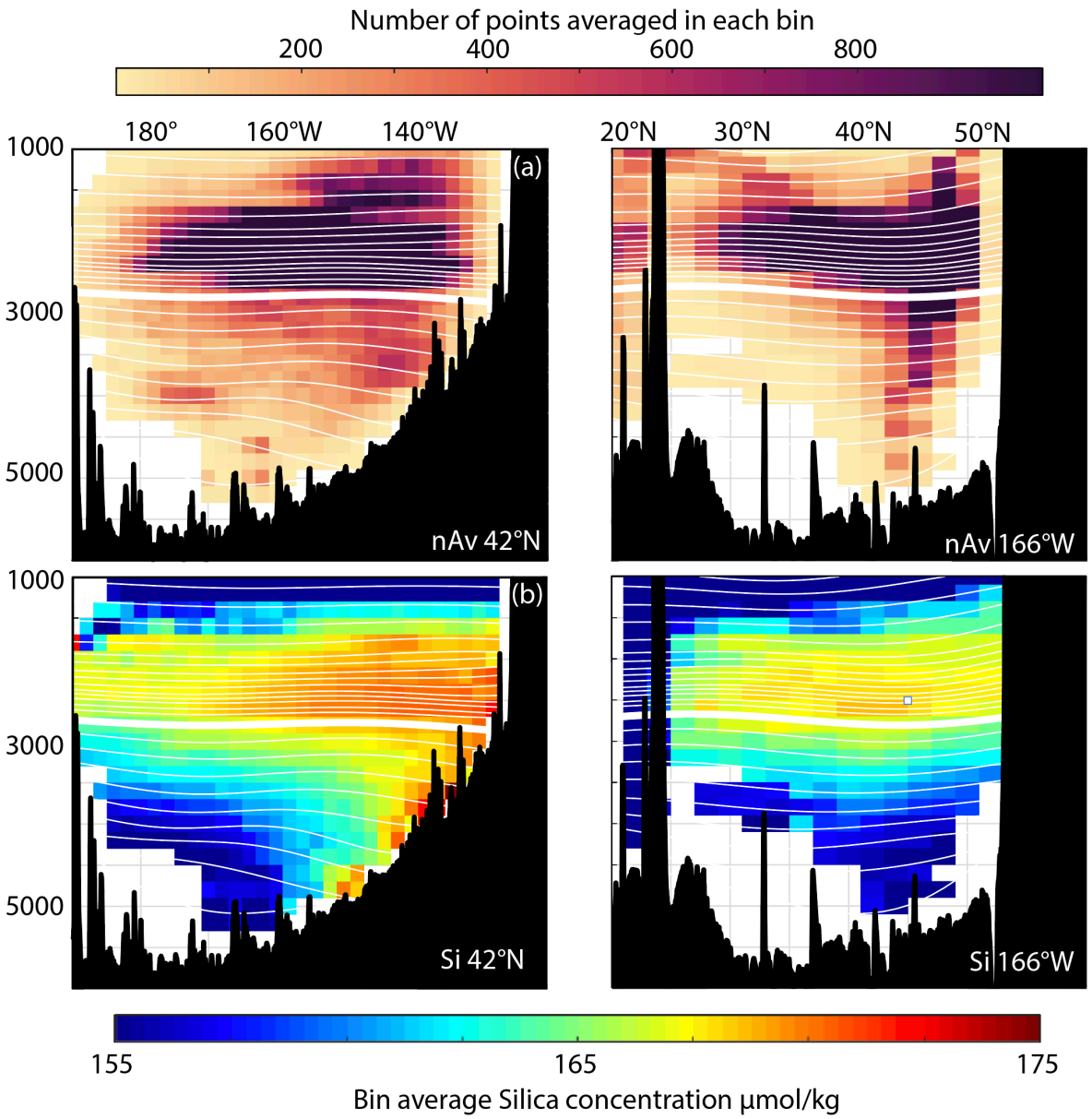

Figure S-D4. Vertical sections (see Figure 1 for comparison) for a 100 realization run where the boundary slippage algorithm is turned off. While the number of points to average for each Eulerian bin decreases, particularly in the UCDW, the double silica maximum still emerges.

-

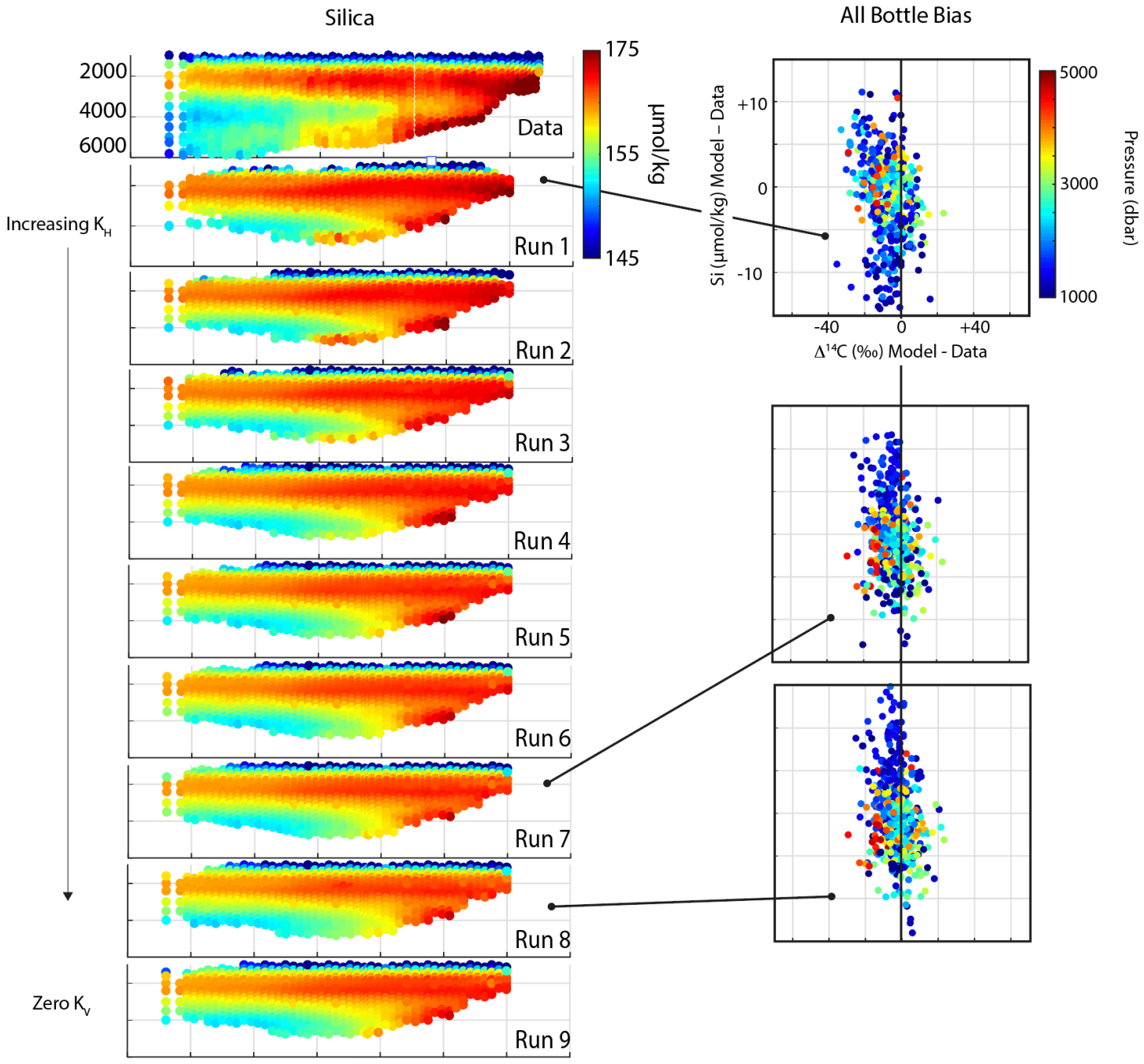

Figure S-D5. Bottle silica concentrations from data along P01-2007 (top, repeated on second page), and for model Runs 1 – 9, with notes indicated along left margin (see Table S-D1). At the right are radiocarbon vs. silica model bias scatter plots for selected runs. The series is continued on the next page.

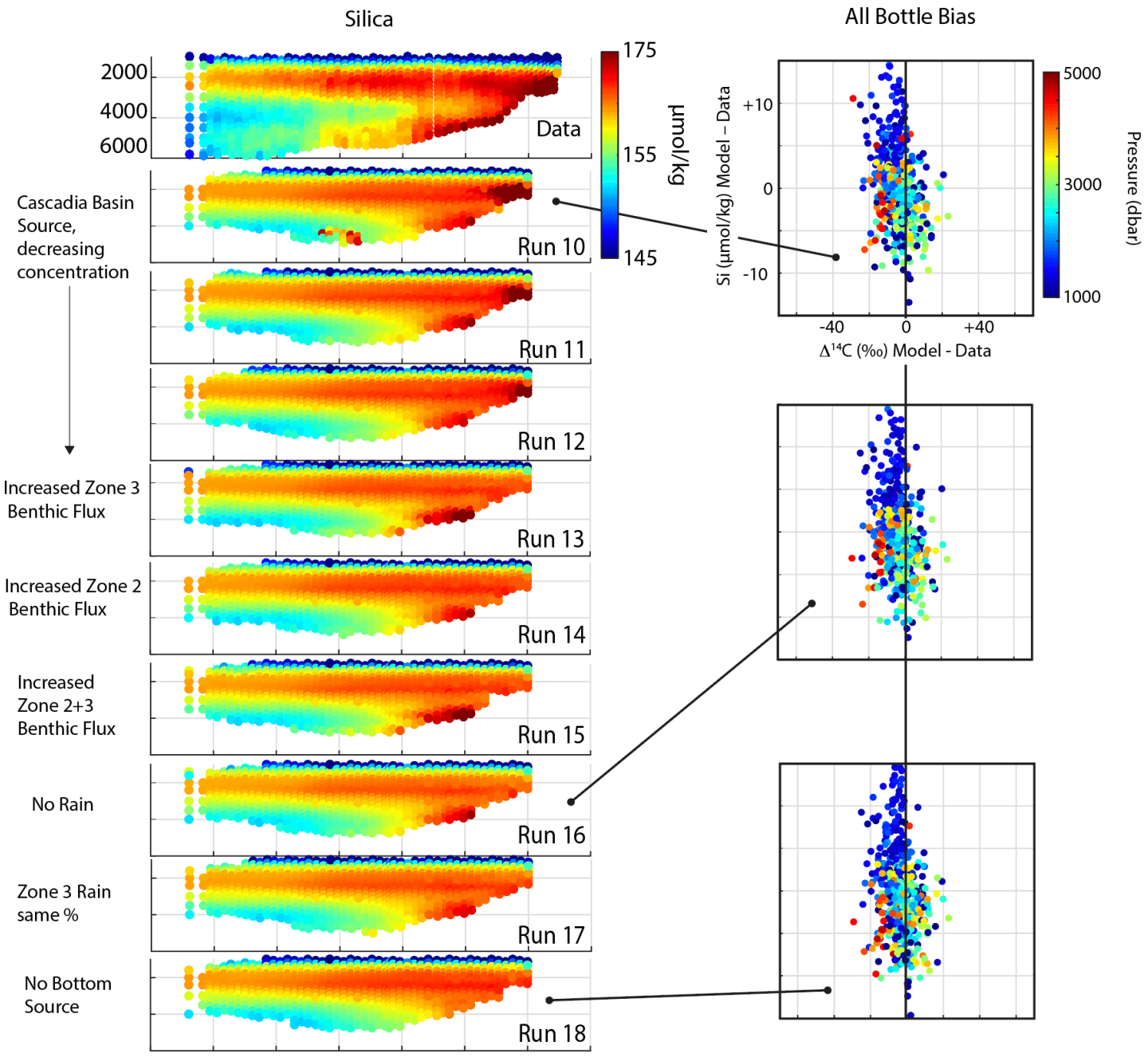

Figure S-D5 (continued). Bottle silica concentrations from data along P01-2007 (top), and for model Runs 10 – 18, with notes indicated along left margin (see Table S-D1). At the right are radiocarbon vs. silica model bias scatter plots for selected runs.